Title
Antisense targeting of decoy exons can reduce intron retention and increase protein expression in human erythroblasts

Journal
RNA, 26(8)

ISSN
1355-8382

Authors
Parra, Marilyn
Zhang, Weiguo
Vu, Jonathan
et al.

Publication Date
2020-08-01

DOI
10.1261/rna.075028.120

Peer reviewed

Antisense targeting of decoy exons can reduce intron retention and increase protein expression in human erythroblasts

Marilyn Parra[1], Weiguo Zhang[1], Jonathan Vu[2], Mark DeWitt[2#], John G. Conboy[1]

[1]Biological Systems and Engineering Division, Lawrence Berkeley National Laboratory, Berkeley, CA, United States

[2]Innovative Genomics Institute, University of California, Berkeley, CA, United States

Correspondence: jgconboy@lbl.gov

[#]Current address: Department of Microbiology, Immunology, & Molecular Genetics, University of California at Los Angeles, Los Angeles, CA, USA

Abstract

The decoy exon model has been proposed to regulate a subset of intron retention (IR) events involving predominantly larger introns (>1kb). Splicing reporter studies have shown that decoy splice sites are essential for activity, suggesting that decoys act by engaging intron-terminal splice sites and competing with cross-intron interactions required for intron excision. The decoy model predicts that antisense oligonucleotides may be able to block decoy splice sites in endogenous pre-mRNA, thereby reducing IR and increasing productive gene expression. Indeed, we now demonstrate that targeting a decoy 5′ splice site in the O-GlcNAc transferase (*OGT*) gene reduced IR from ~80% to ~20% in primary human erythroblasts, accompanied by increases in spliced *OGT* RNA and OGT protein expression. The remaining *OGT* IR was refractory to antisense treatment and might be mediated by independent mechanism(s). In contrast, other retained introns were strongly dependent on decoy function, since antisense targeting of decoy 5′ splice sites greatly reduced (*SNRNP70*) or nearly eliminated (*SF3B1*) IR in two widely expressed splicing factors, and also greatly reduced IR in transcripts encoding the erythroid-specific structural protein, alpha-spectrin (*SPTA1*). These results show that modulating decoy exon function can dramatically alter IR, and suggest that dynamic regulation of decoy exons could be a mechanism to fine tune gene expression post-transcriptionally in many cell types.

Introduction

Gene expression is determined not only by transcription rate, but also by post-transcriptional processes including the efficiency with which pre-mRNA is spliced into translatable mRNA. Intron retention (IR) is a form of RNA processing that selectively modulates splicing of specific introns (Boutz et al. 2015; Braunschweig et al. 2014; Mauger et al. 2016; Jacob and Smith 2017), in essence rendering them ‘alternative introns’. By regulating the efficiency of intron splicing, cells can alter the balance between

two competing pathways: one that generates fully spliced mRNA that can be translated into protein, and a second that produces incompletely spliced "intron retention" transcripts (IR-transcripts). Most of the latter contain premature translation termination signals that preclude synthesis of full length protein. IR-transcripts that are otherwise spliced and polyadenylated can experience several fates in different cellular contexts. Such transcripts are often detained in the nucleus, where they may be degraded (Pendleton et al. 2018) or they may serve as a reservoir for new mRNA production via excision of the retained intron(s) (Boothby et al. 2013; Mauger et al. 2016; Ninomiya et al. 2011); in many cases, the fate is unknown. Alternatively, IR transcripts can be exported to the cytoplasm for degradation by nonsense-mediated decay (NMD) (Wong et al. 2013), or they may persist for translation (Rekosh and Hammarskjold 2018) or other unknown functions (Brugiolo et al. 2017). At a constant transcription rate, greater diversion of pre-mRNA into untranslated IR-transcripts should reduce output of mRNA and decrease protein synthesis. Coordinate regulation of IR can effect programmed changes in gene expression patterns during normal development as cells differentiate and respond to environmental signals (Boutz et al. 2015; Ni et al. 2016; Wong et al. 2013; Mauger et al. 2016; Braun et al. 2017; Naro et al. 2017; Edwards et al. 2016; Pimentel et al. 2016; Shalgi et al. 2014). Conversely, aberrations in the IR program are observed in many diseases including cancers where they can adversely impact expression of many genes (Dvinge and Bradley 2015; Luisier et al. 2018; Adusumalli et al. 2019). Although mechanisms of IR are not well understood, RNA binding proteins (RBPs) (Cho et al. 2014; Pendleton et al. 2017) and factors that modify RBPs (Braun et al. 2017) have been shown impact IR. In a few cases RNA sequence elements required for regulating individual intron retention events have been identified (Park et al. 2017; Pendleton et al. 2017; Rekosh and Hammarskjold 2018; Parra et al. 2018).

Analysis of RNA-seq profiles from differentiating erythroid cell populations revealed highly dynamic, global changes in the erythroid transcriptome, including changes in RNA processing of both cassette

exons and retained introns, as the cells undergo extensive remodeling during the final cell divisions prior to enucleation (An et al. 2014; Pimentel et al. 2014; Pimentel et al. 2016; Edwards et al. 2016). The IR program encompasses hundreds of IR-transcripts that are polyadenylated and spliced except for selective retention of one or more introns (Pimentel et al. 2016; Edwards et al. 2016). In late erythroblasts, numerous IR transcripts are abundantly-expressed, many of which comprise ≥25% of the steady state RNA from their cognate genes. Some of these are dynamically regulated during terminal erythropoiesis, while others exhibit stable IR levels, indicating multiple regulatory pathways (Pimentel et al. 2016). While the majority of erythroblast retained introns are short (<1kb), as observed in other systems (Braunschweig et al. 2014), a subset of important erythroid genes exhibit larger retained introns having embedded decoy exon(s) that are essential for retention (Parra et al. 2018). According to the decoy model, cryptic decoy exon(s) interact nonproductively with intron-terminal splice sites, engaging them in a manner that fails to stimulate efficient splicing catalysis. By competing with cross intron interactions necessary for intron removal, decoy interactions promote IR. Supporting evidence for this model includes the ability of decoy exons to activate IR in heterologous splicing reporters; the dependence of this IR activity on intact decoy splice sites; and the enrichment of U2AF binding at 3' splice sites of decoy exons (Parra et al. 2018).

We explored the hypothesis that antisense targeting of deep intron splice sites, here referring to those associated with decoy exons, can alter endogenous RNA processing fates in primary erythroid progenitors so as to tune gene expression. Previous studies have shown that deep intron splice sites are poorly represented in most RNA-seq datasets, yet they are critical features of recursive splicing pathways that excise selected long introns (Burnette et al. 2005; Hatton et al. 1998; Suzuki et al. 2013; Sibley et al. 2015; Joseph et al. 2018). Deep intron splice sites also have essential functions during catalysis of intermediate steps of nested intrasplicing pathways (Parra et al. 2012; Parra et al. 2008).

Given the ability of antisense oligonucleotides to alter RNA processing outcomes in these pathways by masking deep intron splice sites (Parra et al. 2012; Sibley et al. 2015), we employed a similar strategy to test whether targeting decoy splice sites with antisense reagents can inhibit IR. New results indicate that blocking highly conserved decoy exons in three broadly expressed genes (*SF3B1*, *OGT*, and *SNRNP70*), and in an erythroid-specific gene (*SPTA1*), greatly reduces intron retention activity in endogenous transcripts, and can increase spliced RNA and protein expression. These results validate the function of decoy exons in the context of their natural endogenous transcripts, and suggest that many of the ~400 predicted decoys in differentiating human erythroblasts could be regulated to impact protein expression.

Results

Decoy exon targeting strategy

Candidate decoy exons were identified in retained introns of NMD-inhibited erythroblasts by virtue of the novel splice junctions created when they splice, albeit inefficiently, to adjacent exons (Parra et al. 2018). The decoy model hypothesizes that their main function is to form early spliceosomal complexes with intron-terminal splice sites that become arrested at a pre-catalytic stage of assembly; catalytic splicing at decoy splice sites is inefficient and typically leads to NMD. To assess decoy function in endogenous erythroid transcripts, we reasoned that antisense oligonucleotides targeting decoy exons should interfere with IR to reduce retention efficiency. To maximize our ability to detect such changes, we selected IR-transcripts meeting the following criteria: (1) the transcript must possess a unique intron exhibiting ≥20% retention in late erythroblasts; (2) its cognate gene must be expressed in moderate to high abundance; and (3) the embedded decoy exons must have simple splice site architecture. The last feature served to restrict analysis to decoys that either have unique splice junctions, or have closely

spaced alternative junctions that can be blocked with a single 25nt antisense morpholino (MO). This design was expected to maximize the likelihood of blocking spliceosome assembly at the decoy. However, it eliminated from consideration strong decoys in *ARGLU1* and *DDX39B* that possess alternative splice sites distributed over a wider range (Parra et al. 2018; Pirnie et al. 2017). Finally, we targeted 5' splice sites, because the relatively low GC content at typical 3' splice sites was predicted to reduce MO affinity and effectiveness.

Figure 1A shows relevant features of the IR regions from four genes chosen for analysis. *OGT* intron 4 (3.3kb), *SF3B1* intron 4 (1.8kb), *SNRNP70* intron 7 (3.2kb), and *SPTA1* intron 20 (1.8kb) all exhibit substantial retention in erythroid progenitors at day 9 of the culture (D9) and in well-differentiated erythroblasts at day 16 (D16). Each of these introns encodes decoy exon(s), not represented in Refseq annotations, that were defined by analysis of splice junction reads (Parra et al. 2018) and are depicted in a custom reannotation track (Figure 1A). The decoys in *OGT*, *SF3B1*, and *SNRNP70* have been highly conserved from fish to mammals, while the *SPTA1* decoy is conserved only among mammals. In previous assays with splicing reporters, the *OGT* and *SF3B1* decoys exhibited strong IR activity, while the activity of the *SNRNP70* decoy had weaker activity (Parra et al. 2018). The *SPTA1* decoy has not been assayed previously for IR activity.

The 5' splice site regions of decoys targeted in this study are shown in Figure 1B. The *SF3B1* decoy exhibits only one 5' splice site, while the other three decoys all have alternative 5' splice sites located within 7-12nt of each other. The presence of multiple splice sites could be integral to the decoy mechanism, since this appeared to be a frequent feature of decoy exons, and because it has been shown that concurrent occupancy of alternative splice sites can inhibit splicing (Chen et al. 2017). The shaded regions indicate sequences targeted by antisense morpholinos in the IR assays below.

Reduction of intron retention by antisense targeting of decoy 5' splice sites

Primary human erythroid cultures were electroporated with antisense morpholinos and cultured for two days under standard conditions. RNA was then isolated for analysis by RT-PCR to investigate changes in the balance between IR-transcripts and spliced transcripts. We studied the effects of decoy targeting in four different genes using this approach. The targeting scheme and PCR strategy for analysis of IR in the *OGT* gene, which encodes O-GlcNAC transferase, is shown in Figures 2A. The decoy in *OGT* intron 4 exhibited strong IR activity in minigene splicing reporters (Parra et al. 2018). In endogenous *OGT* transcripts, we first assessed retention of the full length intron 4 by standard RT-PCR analysis under conditions that interrogate the E3-E6 region. Control cells treated with an irrelevant MO yielded two major *OGT* amplification products: a short product representing spliced mRNA, and a larger product corresponding to an IR transcript in which introns 3 and 5 were removed but intron 4 retained (Figure 2B, lane 1). Cells treated with the *OGT* decoy-specific MO exhibited a substantial decrease in the IR isoform (Figure 2B, lane 2). In contrast, the *OGT* MO did not alter retention of a heterologous decoy-containing intron in the *SF3B1* gene, confirming specificity of the MO effects on IR (Figure 2C, compare lanes 1 and 2). These results strongly support the hypothesis that full length introns are specifically retained in a subset of transcripts, and that retention can be greatly suppressed by anti-decoy MOs.

However, standard RT-PCR does not provide a quantitative measure of PIR (percent intron retention), in part due to inefficient amplification of long retained introns. We therefore performed RT-qPCR using primers that amplify unique regions of the IR isoforms or the spliced isoforms, respectively. For *OGT*, the fraction of transcripts bearing the retained intron was estimated at ~80% in control cells, but PIR was substantially reduced to ~21% in cells targeted with the *OGT* decoy 5' splice site MO (Figure 2D). Interestingly, the level of *OGT* IR did not decrease further when the MO concentration was doubled

(results not shown), suggesting that a component of *OGT* IR is modulated in a decoy-independent manner.

The next decoy-mediated IR event selected for analysis was in the *SF3B1* gene (Figure 3A). We focused on decoy exon 4e, shown previously to exhibit the strongest IR activity among several potential decoys in *SF3B1* intron 4 (Parra et al. 2018). Similar to OGT, cells treated with the *SF3B1*-specific MO exhibited much-reduced amounts of the IR-transcript when examined by standard RT-PCR (Figure 3B, compare lanes 1 and 2). Quantitation by qPCR yielded a different result than was observed for *OGT* (Figure 3C), since PIR in controls cells (~26%) was almost eliminated by the *SF3B1* decoy 5' splice site MO (~3%).

The two remaining targets represented decoys about which less prior information was known than for *OGT* and *SF3B1*. The predicted decoy exon in *SNRNP70* is 60/72nt, depending on alternative 5' splice site choice, and might have unique properties since retention has been observed primarily only for downstream intron sequences (Figure 1A). Moreover, this decoy exhibited only weak IR activity in a heterologous splicing reporter (Parra et al. 2018). For *SPTA1*, an 80/87nt noncoding decoy exon mapping near the 3' end of retained intron 20 was predicted on the basis of splice junction reads. A few RNA-seq reads spanned the *SPTA1* decoy exon and linked it to both exon 19 upstream and exon 20 downstream, confirming its potential to be spliced at low frequency (data not shown). Given that *SPTA1* encodes an abundant and erythroid-specific structural protein, alpha spectrin, control of IR could be important in regulating assembly of the erythroid membrane skeleton during terminal erythropoiesis.

Figures 4A and 4B show the targeting approach and PCR strategies used to test IR-promoting activity for predicted decoy exons in *SNRNP70* and *SPTA1*. The effects of decoy-specific antisense MOs were assessed by RT-qPCR to quantitate both IR transcripts and fully spliced transcripts (Figures 4C and 4D).

Electroporation of human erythroblasts with a MO against the 5' splice site region of *SNRNP70*'s decoy substantially reduced the level of IR from about 35% in control erythroid cells to about 9% in MO-treated cells (Figure 4C). Interestingly, the *SPTA1* decoy-specific MO also strongly inhibited IR, from ~20% down to only ~2% (Figure 4D). Together these results strongly support the hypothesis that decoy exons represent a novel regulatory component of the gene expression program, in which they can quantitatively modulate mRNA expression levels by tuning the splicing efficiency of key retained introns.

Impact of decoy targeting on expression of spliced RNA and protein

The dramatic reduction in IR for several genes suggests that inhibition of decoy exon function should lead to increased expression of spliced mRNA and increased capacity for protein synthesis. We explored this issue using *OGT* as a model, since the large MO-induced reduction in PIR would be expected to yield a significant increase in protein expression. Based on the 4-fold difference in IR between control cells and cells treated with the *OGT* decoy-specific MO, measured at 48hrs post-electroporation, one might predict a similar 4-fold increase in *OGT* mRNA and protein. Analysis of qPCR data revealed that the spliced *OGT* transcripts were actually increased 1.7-2.7-fold, when normalized to actin transcript expression in the same cells (Figure 5A). To explore the reason for the modest discrepancy in expected vs observed expression, we quantitated total *OGT* transcript levels (spliced plus IR transcripts) and found that overall *OGT* RNA expression was reduced in comparison to control cells. Therefore, the 4-fold increase in splicing efficiency was partially offset by reduced steady state *OGT* RNA levels, presumably due to other compensatory mechanisms as part of O-GlcNAc homeostasis. Nevertheless, this result confirms that regulation of decoy-mediated IR effected a significant change in spliced *OGT* RNA expression.

Finally, we assessed erythroblast OGT protein expression as a function of variation in IR efficiency. Equal amounts of protein from control MO- or *OGT* MO-treated cells were immunoblotted with anti-OGT antibodies (Figure 5B). Densitometric analysis of OGT expression, normalized to expression of a control protein, GAPDH, revealed ~1.4-fold increase in OGT protein levels in two independent experiments (compare control lanes to *OGT* MO lanes). Interestingly, it has been shown that *OGT* intron retention can also be reduced, and OGT protein expression elevated, by pharmacological treatment of nonerythroid cell lines with the OGT enzyme inhibitors OSMI-1 and OSMI-2 (Park et al. 2017; Tan et al. 2020). This effect has been interpreted as a compensatory mechanism for cells to respond to reduced OGT enzyme activity, i.e., they modify RNA processing pathways so as to reduce *OGT* IR and stimulate production of more total OGT protein. We found that the reducing *OGT* IR independently through the use of decoy-targeting MOs had a similar stimulatory effect on OGT protein expression in erythroblasts (compare Figures 5B and 5C), suggesting that the effects of OSMI-1 may be mediated through the decoy exon mechanism.

Discussion

The decoy exon model proposes that intron retention levels can be controlled by modulating the balance between two competing splice site interactions: (1) productive cross-intron interactions, involving annotated splice sites at the intron termini, that promote splicing catalysis to remove the intron, and (2) nonproductive interactions, involving contacts between internal decoy exon(s) and intron terminal splice sites, that function mainly to block intron excision and promote intron retention. The latter are spliced inefficiently or not at all, presumably due to arrest of spliceosomal assembly at a pre-catalytic complex by mechanisms yet to be defined. The current study validates a major prediction of the decoy hypothesis, namely, that blocking decoy exon function in endogenous pre-mRNA should shift RNA

processing in favor of better intron removal. All four genes targeted with decoy exon 5' splice site-specific antisense MOs were shown to exhibit substantial decreases in IR. Targeting decoy 3' splice sites should in principle also abrogate intron retention, based on experiments with minigene splicing reporters showing that 3' splice site mutations disrupt IR (Parra et al. 2018). However, preliminary experiments with 3' targeting morpholinos thus far have yielded mixed results: all three tested were less effective than the corresponding 5'-targeting reagents, likely due to lower predicted base-pairing affinity and/or undesirable self-complementarity properties of these particular decoy sequences (results not shown). Interestingly, for two genes (*SF3B1* and *SPTA1*), blocking the decoy exon 5' splice site essentially eliminated IR, suggesting that the decoy pathway may be the sole determinant of IR. In contrast, IR was not completely abrogated by antisense treatment in the OGT gene, consistent with the co-existence of decoy-independent IR mechanisms (Monteuuis et al. 2019; Braun et al. 2017; Cho et al. 2014; Wong et al. 2017). Importantly, in the one case tested, *OGT*, decreased IR was accompanied by increases in spliced RNA and protein expression.

The IR transcripts studied here regulate expression of genes with diverse roles in erythropoiesis. Three function in general biochemical processes such as O-GlcNAc homeostasis (*OGT*) and pre-mRNA splicing (*SF3B1* and *SNRNP70*), that are widely important in both erythroid and nonerythroid cells. Presumably the decoy mechanism actively regulates these genes in many different cell types. In contrast, *SPTA1* functions predominantly in erythroid cells where it encodes a major structural component of the membrane skeleton that mechanical supports the eventual red cell membrane. Given the measured PIR values of 25-75% in these genes, full inhibition of IR could lead to 1.3-4-fold increases in protein expression, with most genes capable of ≤2-fold changes based on these bulk measures of IR. We speculate that the major purpose of decoy-mediated IR may be fine tuning of expression according to the cell's physiological needs. In fact, IR has already been shown to tune OGT expression in cancer cell

lines via an intronic element (Park et al. 2017) that likely operates via the decoy mechanism. For *SPTA1*, decoy-mediated intron retention could function in a similar manner to balance expression of the alpha and beta spectrin chains, two high molecular weight proteins that form an extended heterodimer that assembles into higher order structures supporting the red cell membrane. An imbalance of spectrin chains might be detrimental to human erythroblasts, and control of IR could serve to equalize the cellular content of these binding partner proteins. Finally, differentiating erythroblasts might dynamically regulate IR for splicing factor genes so that RNA splicing capacity could adapt to changes pre-mRNA abundance as thousands of genes are down-regulated during terminal erythropoiesis (An et al. 2014).

Interestingly, global comparison of RNA and protein abundance profiles in differentiating human erythroblasts has revealed discordant expression patterns that can be explained in part by IR (Gautier et al. 2016). Profiling experiments have shown that genes displaying increased RNA levels but decreased protein expression, as cells progressively differentiate into late stage erythroblasts, are enriched in IR-transcripts. In such cases IR may function to down-regulate productive gene expression in a post-transcriptional manner. We propose that decoy-mediated IR contributes substantially to this phenomenon, since erythroblasts express an estimated 400 retained introns embedded with candidate decoy exon(s) (Parra et al. 2018). Moreover, the number of functional decoys could be greater, because many of intronic U2AF binding sites detected in K562 cells do not align with splice junction-predicted erythroblast decoy exons. These U2AF sites of unknown function, perhaps regulated by novel RBP cofactors (Sutandy et al. 2018), could represent ‘silent’ decoys that promote IR without being catalytically spliced. Preliminary experiments supporting this idea are under further investigation.

The discovery of decoy exons provides new evidence that many unannotated splicing elements reside in deep intron space, hundreds to many thousands of nucleotides from the regulated splice sites, and that

they play essential roles in regulating proper splice patterns via several mechanisms (Ule and Blencowe 2019). The decoy model discussed here is presumably employed in diverse cell types, since many decoy-containing introns are retained in a wide range of non-erythroid cell types. Another mechanism dependent on deep intron splicing elements is recursive splicing (RS). RS involves functional recognition of RS-exons, embedded deep within long introns, as critical splicing intermediates (Sibley et al. 2015; Joseph et al. 2018). Finally, a mechanism termed intrasplicing requires deep intron splicing elements, located tens of kilobases upstream of the regulated splice acceptors, to promote nested splicing reactions required for proper splice site selection in two paralogs of the protein 4.1 gene family (Parra et al. 2008; Parra et al. 2012). In various contexts, antisense oligonucleotides that block deep intron elements have been used to demonstrate their functional importance in splicing of endogenous pre-mRNAs (Parra et al. 2012; Sibley et al. 2015; Lovci et al. 2013).

Finally, the current results suggest new clinical applications of antisense reagents for the purpose of improving gene expression. Pioneering work more than 20 years ago showed that antisense oligonucleotides can block aberrant splice sites to restore correct splicing of the erythroid β-globin gene in thalassemic pre-mRNA (Dominski and Kole 1993). Since that time an increasing array of antisense strategies has been utilized to increase proper gene expression by manipulating RNA processing. Antisense oligonucleotides can induce exon skipping in dystrophin pre-mRNA to restore the translational reading frame in patients with Duchenne muscular dystrophy (e.g., (Aartsma-Rus and Krieg 2017)); they can mask intronic splicing silencer(s) downstream of *SMN2* exon 7 to improve productive splicing in patients with spinal muscular atrophy (Bennett et al. 2019); and, given increasing evidence that deep intron mutations can cause human disease (Vaz-Drago et al. 2017), antisense reagents can also improve gene expression by blocking deep intron splicing mutations that activate inclusion of cryptic noncoding exons in the breast cancer gene *BRCA2* (Anczukow et al. 2012) and the

deaf-blindness gene *USH2A* (Slijkerman et al. 2016). As mentioned in the introduction, antisense reagents can mask deep intron splice sites so as to modulate RNA processing during recursive splicing and intrasplicing (Parra et al. 2012; Sibley et al. 2015). Antisense reagents can even increase productive gene expression by inhibiting nonsense-mediated mRNA decay (Nomakuchi et al. 2016). Here we have shown that antisense oligonucleotides can increase protein expression by blocking decoy splice sites in retained introns, which could allow a functional allele to increase protein output to compensate for genetic deficiencies in various disease states. Relevant disease phenotypes may arise due to haploinsufficiency or, as in the case of hereditary spherocytosis associated with α-spectrin deficiency, they may be due to biallelic *SPTA1* mutations (Chonat et al. 2019), some of which induce aberrant splicing by activating distal branch points (Gallagher et al. 2019). Since disease severity correlates with the level of α-spectrin protein in the patient's red blood cell cytoskeleton (Chonat et al. 2019), blocking decoy-mediated IR in *SPTA1* could have therapeutic value.

Materials and Methods

Erythroblast culture. CD34+ erythroid progenitors were enriched from cord blood and cultured under conditions previously shown to support selective growth and differentiation of erythroid cells (Hu et al. 2013). For electroporation, 10^6 erythroblasts at day 11 of culture were electroporated at room temperature in supplemented P3 solution using a Lonza 4D-Nucleofector system with the ER 100 pulse code. 25nt morpholinos, antisense to the regions highlighted in Figure 1B, were obtained from Gene Tools LLC (Philomath, OR), maintained in sterile saline solution, and added to the cells at 30μM final concentration just prior to electroporation. After electroporation cells were incubated in culture medium at 37˚C for 2 days before further processing. When RNA and protein were isolated from the same sample, ~$2.5x10^5$ cells were used for the RNA preparation and $7.5x10^5$ cells for protein purification. Morpholino sequences antisense to the 5' splice sites of the targeted decoys were as follows:

OGT, 5'-gtggcagttacaaac|ccgttac|CAT-3';

SPTA1, 5'-ctggctggaac|ctcttac|GTGGCTG-3';

SF3B1, 5'-atccggaatacgtac|ACTTTCGTGC-3';

SNRNP70, 5'-ccatgatac|aaac|CCTTATACCAAC-3'.

Sequences antisense to the intron are in lower case; sequences antisense to the exon are in upper case; EXON|intron boundaries are marked by vertical lines.

RT-PCR. Total RNA was extracted from human erythroid progenitors and analyzed by standard RT-PCR methods as described (Pimentel et al. 2016). For quantitative analysis, RT-qPCR was performed using an Applied Biosystems 7500 Fast Real-Time PCR System with Quanta SYBR Green Fastmix low ROX reagents. The SYBR Green buffers were supplemented with forward and reverse primers at a final concentration of 0.5μM, and the spliced RNA or IR-RNA DNAs amplified using the following program: initial denaturation (1 cycle): 94°C for 15 min; amplification stage (40 cycles): 95°C for 10 sec, 60°C for 25 sec, and 72°C for 30 sec; final extension at 72°C for 30 sec. Size and identity of qPCR products (Table 1) were confirmed by gel electrophoresis (Figure S1) and by DNA sequencing. The relative expression of each gene was calculated using the comparative ΔCt method after normalizing to the ACTB control.

Western blot analysis. After electroporation followed by an additional ~48hrs of culture, an estimated $7.5x10^5$ cells were pelleted and stored at -80˚C. Protein was subsequently isolated from lysed cells, subjected to SDS-polyacrylamide gel electrophoresis, and immunoblotted using rabbit polyclonal antibody against OGT (Proteintech group, Inc., Rosemont, IL; cat. no. 11576-2) at 1:4000 dilution, or rabbit polyclonal antibody against GAPDH (Sigma, cat.no. G9545) at 1:10,000 dilution.

Acknowledgments

This work was funded by National Institutes of Health grant 5R01DK108020 (J.G.C.) and by the Director, Office of Science and Office of Biological & Environmental Research of the US Department of Energy (DE-AC02-05CH1123).

References

Aartsma-Rus, A. and A. M. Krieg (2017). FDA Approves Eteplirsen for Duchenne Muscular Dystrophy: The Next Chapter in the Eteplirsen Saga. *Nucleic Acid Ther* **27**: 1-3.

Adusumalli, S., Z. K. Ngian, W. Q. Lin, T. Benoukraf and C. T. Ong (2019). Increased intron retention is a post-transcriptional signature associated with progressive aging and Alzheimer's disease. *Aging Cell* **18**: e12928.

An, X., V. P. Schulz, J. Li, K. Wu, J. Liu, F. Xue, J. Hu, N. Mohandas and P. G. Gallagher (2014). Global transcriptome analyses of human and murine terminal erythroid differentiation. *Blood* **123**: 3466-3477.

Anczukow, O., M. Buisson, M. Leone, C. Coutanson, C. Lasset, A. Calender, O. M. Sinilnikova and S. Mazoyer (2012). BRCA2 deep intronic mutation causing activation of a cryptic exon: opening toward a new preventive therapeutic strategy. *Clin Cancer Res* **18**: 4903-4909.

Bennett, C. F., A. R. Krainer and D. W. Cleveland (2019). Antisense Oligonucleotide Therapies for Neurodegenerative Diseases. *Annu Rev Neurosci* **42**: 385-406.

Boothby, T. C., R. S. Zipper, C. M. van der Weele and S. M. Wolniak (2013). Removal of retained introns regulates translation in the rapidly developing gametophyte of Marsilea vestita. *Dev Cell* **24**: 517-529.

Boutz, P. L., A. Bhutkar and P. A. Sharp (2015). Detained introns are a novel, widespread class of post-transcriptionally spliced introns. *Genes Dev* **29**: 63-80.

Braun, C. J., M. Stanciu, P. L. Boutz, J. C. Patterson, D. Calligaris, F. Higuchi, R. Neupane, S. Fenoglio, D. P. Cahill, H. Wakimoto, et al. (2017). Coordinated Splicing of Regulatory Detained Introns

within Oncogenic Transcripts Creates an Exploitable Vulnerability in Malignant Glioma. *Cancer Cell* **32**: 411-426 e411.

Braunschweig, U., N. L. Barbosa-Morais, Q. Pan, E. N. Nachman, B. Alipanahi, T. Gonatopoulos-Pournatzis, B. Frey, M. Irimia and B. J. Blencowe (2014). Widespread intron retention in mammals functionally tunes transcriptomes. *Genome Res* **24**: 1774-1786.

Brugiolo, M., V. Botti, N. Liu, M. Muller-McNicoll and K. M. Neugebauer (2017). Fractionation iCLIP detects persistent SR protein binding to conserved, retained introns in chromatin, nucleoplasm and cytoplasm. *Nucleic Acids Res* **45**: 10452-10465.

Burnette, J. M., E. Miyamoto-Sato, M. A. Schaub, J. Conklin and A. J. Lopez (2005). Subdivision of large introns in Drosophila by recursive splicing at nonexonic elements. *Genetics* **170**: 661-674.

Chen, L., R. Weinmeister, J. Kralovicova, L. P. Eperon, I. Vorechovsky, A. J. Hudson and I. C. Eperon (2017). Stoichiometries of U2AF35, U2AF65 and U2 snRNP reveal new early spliceosome assembly pathways. *Nucleic Acids Res* **45**: 2051-2067.

Cho, V., Y. Mei, A. Sanny, S. Chan, A. Enders, E. M. Bertram, A. Tan, C. C. Goodnow and T. D. Andrews (2014). The RNA-binding protein hnRNPLL induces a T cell alternative splicing program delineated by differential intron retention in polyadenylated RNA. *Genome Biol* **15**: R26.

Chonat, S., M. Risinger, H. Sakthivel, O. Niss, J. A. Rothman, L. Hsieh, S. T. Chou, J. L. Kwiatkowski, E. Khandros, M. F. Gorman, et al. (2019). The Spectrum of SPTA1-Associated Hereditary Spherocytosis. *Front Physiol* **10**: 815.

Dominski, Z. and R. Kole (1993). Restoration of correct splicing in thalassemic pre-mRNA by antisense oligonucleotides. *Proc Natl Acad Sci U S A* **90**: 8673-8677.

Dvinge, H. and R. K. Bradley (2015). Widespread intron retention diversifies most cancer transcriptomes. *Genome Med.* **7**: 45.

Edwards, C. R., W. Ritchie, J. J. Wong, U. Schmitz, R. Middleton, X. An, N. Mohandas, J. E. Rasko and G. A. Blobel (2016). A dynamic intron retention program in the mammalian megakaryocyte and erythrocyte lineages. *Blood* **127**: e24-e34.

Gallagher, P. G., Y. Maksimova, K. Lezon-Geyda, P. E. Newburger, D. Medeiros, R. D. Hanson, J. Rothman, S. Israels, D. A. Wall, R. F. Sidonio, Jr., et al. (2019). Aberrant splicing contributes to severe alpha-spectrin-linked congenital hemolytic anemia. *J Clin Invest* **129**: 2878-2887.

Gautier, E. F., S. Ducamp, M. Leduc, V. Salnot, F. Guillonneau, M. Dussiot, J. Hale, M. C. Giarratana, A. Raimbault, L. Douay, et al. (2016). Comprehensive Proteomic Analysis of Human Erythropoiesis. *Cell Rep* **16**: 1470-1484.

Hatton, A. R., V. Subramaniam and A. J. Lopez (1998). Generation of alternative Ultrabithorax isoforms and stepwise removal of a large intron by resplicing at exon-exon junctions. *Mol Cell* **2**: 787-796.

Hu, J., J. Liu, F. Xue, G. Halverson, M. Reid, A. Guo, L. Chen, A. Raza, N. Galili, J. Jaffray, et al. (2013). Isolation and functional characterization of human erythroblasts at distinct stages: implications for understanding of normal and disordered erythropoiesis in vivo. *Blood* **121**: 3246-3253.

Jacob, A. G. and C. W. J. Smith (2017). Intron retention as a component of regulated gene expression programs. *Hum Genet* **136**: 1043-1057.

Joseph, B., S. Kondo and E. C. Lai (2018). Short cryptic exons mediate recursive splicing in Drosophila. *Nat Struct Mol Biol* **25**: 365-371.

Lovci, M. T., D. Ghanem, H. Marr, J. Arnold, S. Gee, M. Parra, T. Y. Liang, T. J. Stark, L. T. Gehman, S. Hoon, et al. (2013). Rbfox proteins regulate alternative mRNA splicing through evolutionarily conserved RNA bridges. *Nat Struct Mol Biol* **20**: 1434-1442.

Luisier, R., G. E. Tyzack, C. E. Hall, J. S. Mitchell, H. Devine, D. M. Taha, B. Malik, I. Meyer, L. Greensmith, J. Newcombe, et al. (2018). Intron retention and nuclear loss of SFPQ are molecular hallmarks of ALS. *Nat Commun* **9**: 2010.

Mauger, O., F. Lemoine and P. Scheiffele (2016). Targeted Intron Retention and Excision for Rapid Gene Regulation in Response to Neuronal Activity. *Neuron* **92**: 1266-1278.

Monteuuis, G., J. J. L. Wong, C. G. Bailey, U. Schmitz and J. E. J. Rasko (2019). The changing paradigm of intron retention: regulation, ramifications and recipes. *Nucleic Acids Res* **47**: 11497-11513.

Naro, C., A. Jolly, S. Di Persio, P. Bielli, N. Setterblad, A. J. Alberdi, E. Vicini, R. Geremia, P. De la Grange and C. Sette (2017). An Orchestrated Intron Retention Program in Meiosis Controls Timely Usage of Transcripts during Germ Cell Differentiation. *Dev Cell* **41**: 82-93 e84.

Ni, T., W. Yang, M. Han, Y. Zhang, T. Shen, H. Nie, Z. Zhou, Y. Dai, Y. Yang, P. Liu, et al. (2016). Global intron retention mediated gene regulation during CD4+ T cell activation. *Nucleic Acids Res* **44**: 6817-6829.

Ninomiya, K., N. Kataoka and M. Hagiwara (2011). Stress-responsive maturation of Clk1/4 pre-mRNAs promotes phosphorylation of SR splicing factor. *J Cell Biol* **195**: 27-40.

Nomakuchi, T. T., F. Rigo, I. Aznarez and A. R. Krainer (2016). Antisense oligonucleotide-directed inhibition of nonsense-mediated mRNA decay. *Nat Biotechnol* **34**: 164-166.

Park, S. K., X. Zhou, K. E. Pendleton, O. V. Hunter, J. J. Kohler, K. A. O'Donnell and N. K. Conrad (2017). A Conserved Splicing Silencer Dynamically Regulates O-GlcNAc Transferase Intron Retention and O-GlcNAc Homeostasis. *Cell Rep* **20**: 1088-1099.

Parra, M., B. W. Booth, R. Weiszmann, B. Yee, G. W. Yeo, J. B. Brown, S. E. Celniker and J. G. Conboy (2018). An important class of intron retention events in human erythroblasts is regulated by cryptic exons proposed to function as splicing decoys. *RNA* **24**: 1255-1265.

Parra, M. K., T. L. Gallagher, S. L. Amacher, N. Mohandas and J. G. Conboy (2012). Deep intron elements mediate nested splicing events at consecutive AG-dinucleotides to regulate alternative 3' splice site choice in vertebrate 4.1 genes. *Mol Cell Biol* **32**: 2044-2053.

Parra, M. K., J. S. Tan, N. Mohandas and J. G. Conboy (2008). Intrasplicing coordinates alternative first exons with alternative splicing in the protein 4.1R gene. *EMBO J* **27**: 122-131.

Pendleton, K. E., B. Chen, K. Liu, O. V. Hunter, Y. Xie, B. P. Tu and N. K. Conrad (2017). The U6 snRNA m(6)A Methyltransferase METTL16 Regulates SAM Synthetase Intron Retention. *Cell* **169**: 824-835 e814.

Pendleton, K. E., S. K. Park, O. V. Hunter, S. M. Bresson and N. K. Conrad (2018). Balance between MAT2A intron detention and splicing is determined cotranscriptionally. *RNA* **24**: 778-786.

Pimentel, H., M. Parra, S. Gee, D. Ghanem, X. An, J. Li, N. Mohandas, L. Pachter and J. G. Conboy (2014). A dynamic alternative splicing program regulates gene expression during terminal erythropoiesis. *Nucleic Acids Res* **42**: 4031-4042.

Pimentel, H., M. Parra, S. L. Gee, N. Mohandas, L. Pachter and J. G. Conboy (2016). A dynamic intron retention program enriched in RNA processing genes regulates gene expression during terminal erythropoiesis. *Nucleic Acids Res* **44**: 838-851.

Pirnie, S. P., A. Osman, Y. Zhu and G. G. Carmichael (2017). An Ultraconserved Element (UCE) controls homeostatic splicing of ARGLU1 mRNA. *Nucleic Acids Res* **45**: 3473-3486.

Rekosh, D. and M. L. Hammarskjold (2018). Intron retention in viruses and cellular genes: Detention, border controls and passports. *Wiley Interdiscip Rev RNA* **9**: e1470.

Shalgi, R., J. A. Hurt, S. Lindquist and C. B. Burge (2014). Widespread inhibition of posttranscriptional splicing shapes the cellular transcriptome following heat shock. *Cell Rep* **7**: 1362-1370.

Sibley, C. R., W. Emmett, L. Blazquez, A. Faro, N. Haberman, M. Briese, D. Trabzuni, M. Ryten, M. E. Weale, J. Hardy, et al. (2015). Recursive splicing in long vertebrate genes. *Nature* **521**: 371-375.

Slijkerman, R. W., C. Vache, M. Dona, G. Garcia-Garcia, M. Claustres, L. Hetterschijt, T. A. Peters, B. P. Hartel, R. J. Pennings, J. M. Millan, et al. (2016). Antisense Oligonucleotide-based Splice

Correction for USH2A-associated Retinal Degeneration Caused by a Frequent Deep-intronic Mutation. *Mol Ther Nucleic Acids* **5**: e381.

Sutandy, F. X. R., S. Ebersberger, L. Huang, A. Busch, M. Bach, H.-S. Kang, J. Fallmann, D. Maticzka, R. Backofen, P. F. Stadler, et al. (2018). In vitro iCLIP-based modeling uncovers how the splicing factor U2AF2 relies on regulation by cofactors. *Genome Research* **28**: 699-713.

Suzuki, H., T. Kameyama, K. Ohe, T. Tsukahara and A. Mayeda (2013). Nested introns in an intron: evidence of multi-step splicing in a large intron of the human dystrophin pre-mRNA. *FEBS Lett* **587**: 555-561.

Tan, Z.-W., G. Fei, J. A. Paulo, S. Bellaousov, S. E. S. Martin, D. Y. Duveau, C. J. Thomas, S. P. Gygi, P. L. Boutz and S. Walker (2020). O-GlcNAc regulates gene expression by controlling detained intron splicing. *bioRxiv* doi: 10.1101/2020.03.27.012781.

Ule, J. and B. J. Blencowe (2019). Alternative Splicing Regulatory Networks: Functions, Mechanisms, and Evolution. *Mol Cell* **76**: 329-345.

Vaz-Drago, R., N. Custodio and M. Carmo-Fonseca (2017). Deep intronic mutations and human disease. *Hum Genet* **136**: 1093-1111.

Wong, J. J., D. Gao, T. V. Nguyen, C. T. Kwok, M. van Geldermalsen, R. Middleton, N. Pinello, A. Thoeng, R. Nagarajah, J. Holst, et al. (2017). Intron retention is regulated by altered MeCP2-mediated splicing factor recruitment. *Nat Commun* **8**: 15134.

Wong, J. J., W. Ritchie, O. A. Ebner, M. Selbach, J. W. Wong, Y. Huang, D. Gao, N. Pinello, M. Gonzalez, K. Baidya, et al. (2013). Orchestrated intron retention regulates normal granulocyte differentiation. *Cell* **154**: 583-595.

Figure Legends

Figure 1. Intron retention and candidate decoy exons in targeted erythroid genes. 1A. Annotation of key features in IR regions of four prominent erythroid genes. Top panel: Refseq gene annotations, lacking indications of intron retention isoforms or decoy exons predicted within the introns. For SF3B1, only the four frequently spliced decoys are shown, from a total six total (Parra et al. 2018). Lower panels show a reannotation that includes predicted decoy exons (boxed), RNA-seq data from early stage (D9) and late stage (D15) erythroblasts, and phylogenetic conservation of the relevant gene regions. 1B. 5' splice site features of targeted decoy exons. Upper case, decoy exon sequence; lower case, downstream intron sequence. Vertical bars show 5' splice site junctions identified in RNA-seq data from erythroblasts inhibited for nonsense-mediated decay. Shaded regions indicate regions targeted by antisense morpholinos.

Figure 2. Antisense inhibition of *OGR* IR. A. *OGT* gene structure in the IR region showing retained intron 4 (thick gray line) with its decoy exon and flanking exons. Position of antisense MO designed to block the 5' splice site is shown, along with primer pairs used for RT-PCR. B. Gel analysis of IR and spliced bands amplified from endogenous *OGT* transcripts by standard RT-PCR from cells treated with negative control MO (lane 1) or *OGT* decoy-specific MO (lane 2). C. As a control for decoy-specific effects of the MO treatment, gel analysis of IR and spliced bands amplified from endogenous SF3B1 transcripts after treatment with negative control MO (lane 1) or *OGT* decoy-specific MO (lane 2). D. OGT IR, as a percentage of total *OGT* transcripts, in cells treated with negative control or decoy-specific MO. IR was assessed using RT-qPCR. Results show average IR from data of four experiments. Error bars indicate standard deviation.

Figure 3. Antisense inhibition of *SF3B1* IR. A. *SF3B1* gene structure in the IR region showing retained intron 4 (thick gray line) and its major decoy exon, together with adjacent introns and exons. Position of antisense MO designed to block the 5' splice site is shown, along with primer pairs used for RT-PCR. B. Gel analysis of IR and spliced bands amplified from endogenous *SF3B1* transcripts by standard RT-PCR from cells treated with negative control MO (lane 1) or *SF3B1* decoy-specific MO (lane 2). C. *SF3B1* IR, as a percentage of total *SF3B1* transcripts, in cells treated with negative control or decoy-specific MO. IR was assessed using RT-qPCR to compare the relative amounts of IR and spliced products. Results show average IR of three experiments. Error bars indicate standard deviation.

Figure 4. Antisense inhibition of *SNRNP70* IR and *SPTA1* IR. A. *SNRNP70* gene structure in the IR region showing retained intron 7 (thick gray line) with its major decoy exon, together with adjacent introns and exons. Position of antisense MO designed to block the 5' splice site is shown, along with primer pairs used for RT-PCR. B. *SPTA1* gene structure in the IR region showing retained intron 20 (thick gray line) with its major decoy exon, together with adjacent introns and exons. Position of antisense MO designed to block the 5' splice site is shown, along with primer pairs used for RT-PCR. C and D. IR in cells treated with *SNRNP70*-specific (C) or *SPTA1*-specific (D) MO, in parallel with cells subjected to control MO treatment. IR was assessed using RT-qPCR to compare the relative amounts of IR and spliced products.

Figure 5. Decoy inhibition increases spliced RNA and protein output. A. Expression of spliced *OGT* transcript in decoy-inhibited cells, relative to expression in cells treated with a negative control MO. B. OGT protein expression in two independent experiments was increased in cells treated with the *OGT* 5' decoy MO, compared to cells treated with a control MO. GAPDH expression was used to normalize

protein loading. In both experiments inhibition of IR was accompanied by ~1.4-fold increase in protein expression. C. OGT protein expression in two independent experiments was increased in cells treated with the OGT inhibitor OSMI-1, compared to cells treated with buffer alone.

Figure S1. Gel analysis of qPCR products. Amplification products representing each of the major qPCR reactions for spliced (spl) and IR-transcripts (IR) were analyzed by polyacrylamide gel electrophoresis. Designations below the gel indicate well numbers from the 96 well plate used for amplification. Numbers at the left indicate DNA size standards in nucleotides.

Figure 1A

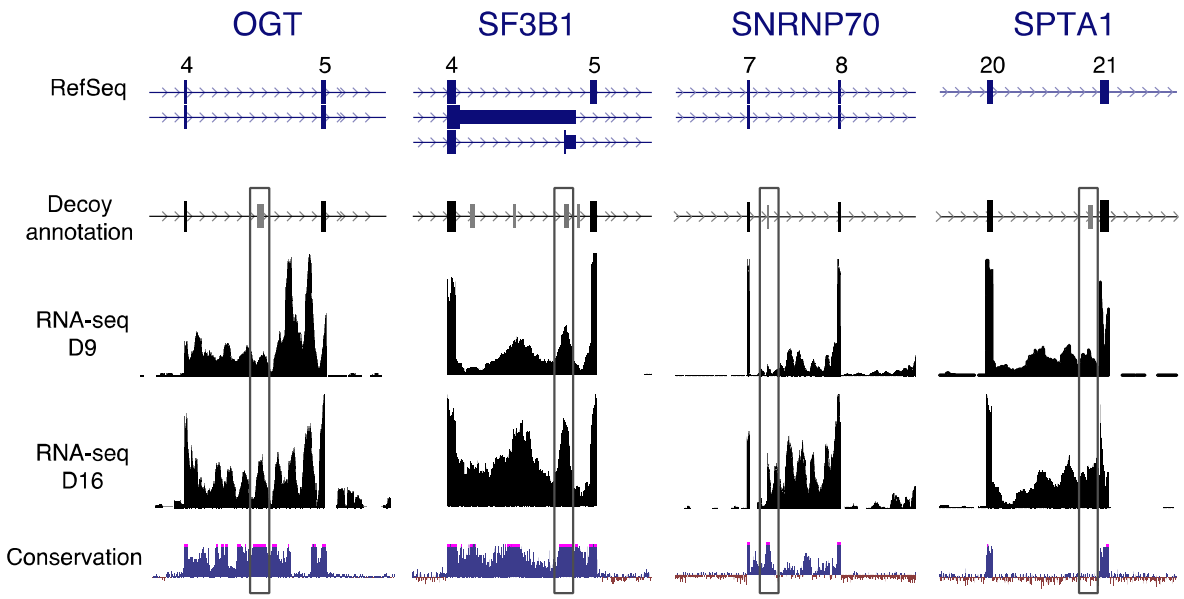

Figure 1B

	decoy exon	5′	5′
OGT	…TCACATGATGAGAAATATG	gtaacgg	gtttgtaactgccacagc
SF3B1	…GAGACAAAGGCACGAAAGT	gtacgtattccggattagcaacccag	
SNRNP70	…TACAACACCTCAGTGTATG	gttggtataagg	gtttgtatcatgg
SPTA1	…CTTTAATCTCTGCAGCCAC	gtaagag	gttccagccagaggctct

Figure 2

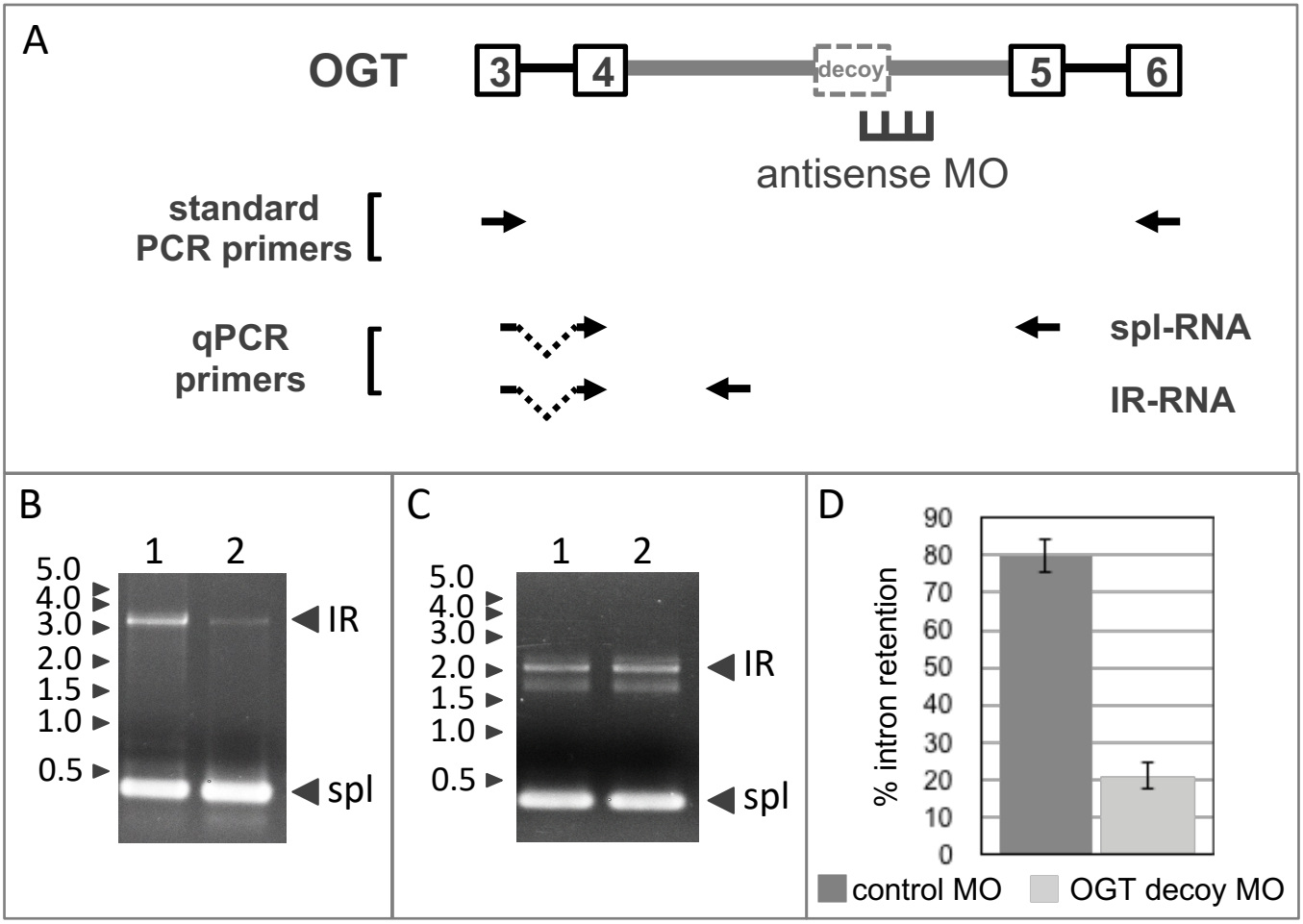
A
OGT
3
4
decoy
5
6
antisense MO
standard
PCR primers
qPCR
primers
spl-RNA
IR-RNA
B
1
2
5.0
4.0
3.0
2.0
1.5
1.0
0.5
IR
spl
C
1
2
5.0
4.0
3.0
2.0
1.5
1.0
0.5
IR
spl
D
% intron retention
90
80
70
60
50
40
30
20
10
0
control MO
OGT decoy MO

Figure 3

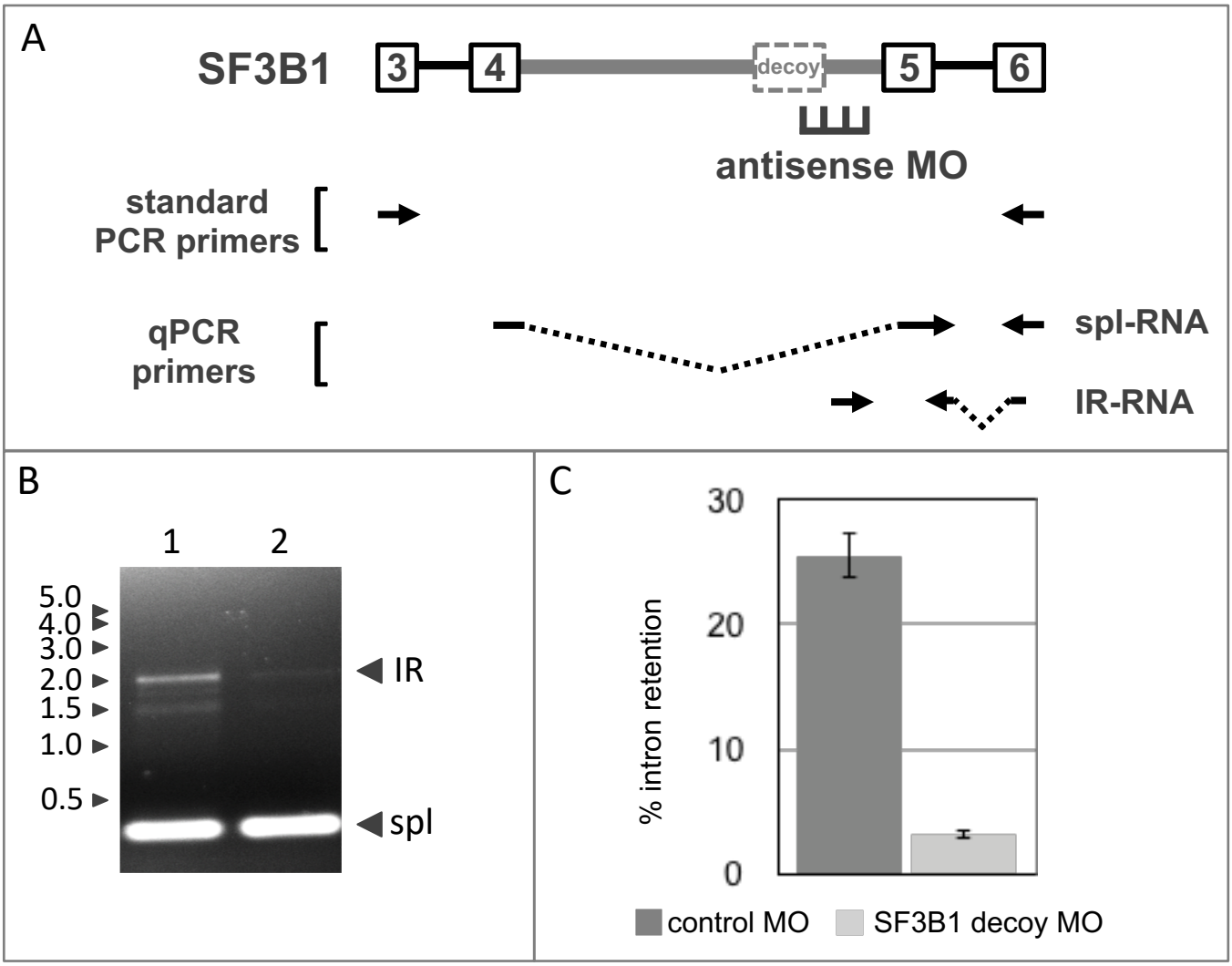
A
SF3B1
3
4
decoy
5
6
antisense MO
standard
PCR primers
qPCR
primers
spl-RNA
IR-RNA
B
1
2
5.0
4.0
3.0
2.0
1.5
1.0
0.5
IR
spl
C
30
20
10
0
% intron retention
control MO
SF3B1 decoy MO

Figure 4

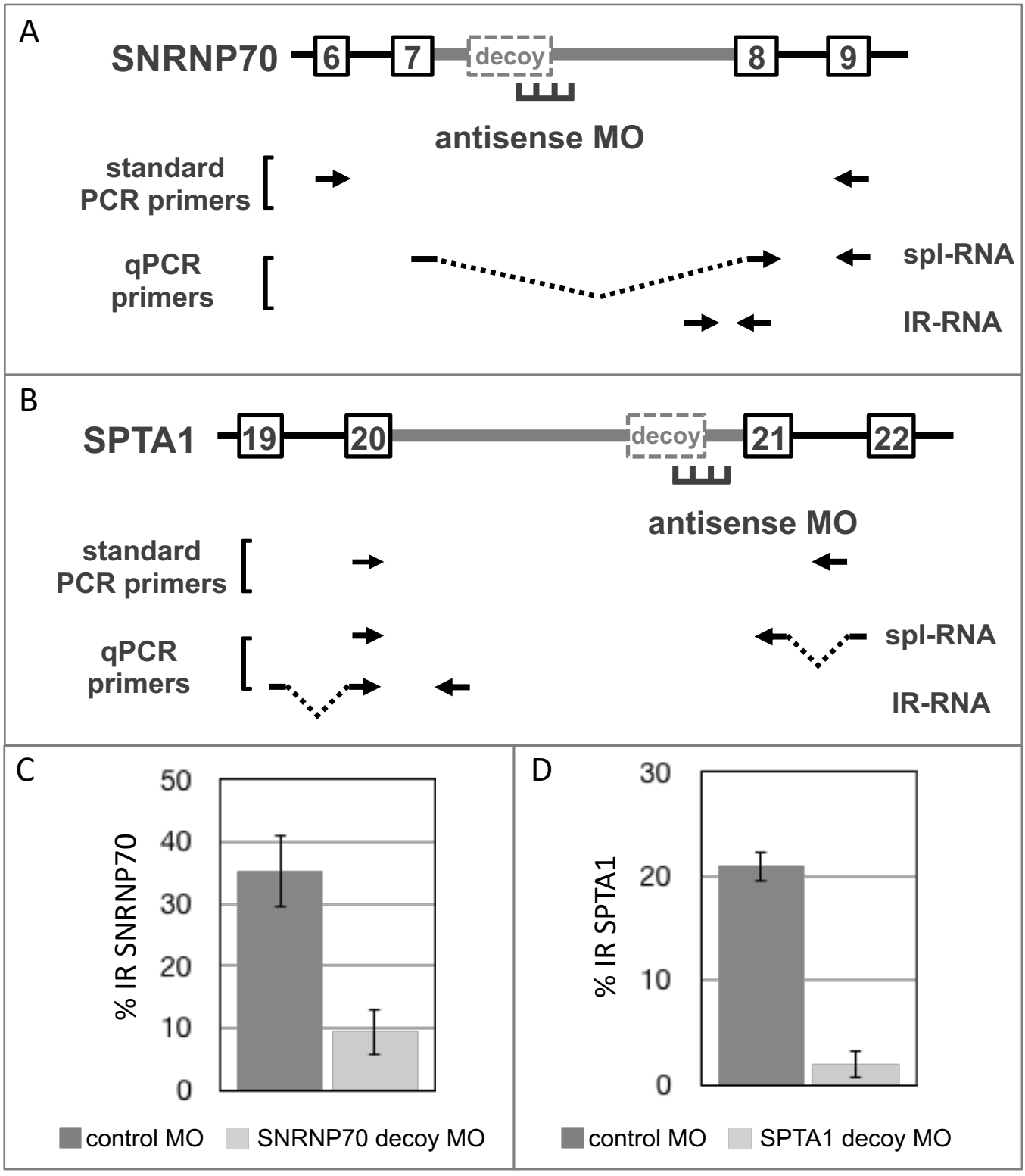
A
SNRNP70
6
7
decoy
8
9
antisense MO
standard PCR primers
qPCR primers
spl-RNA
IR-RNA
B
SPTA1
19
20
decoy
21
22
antisense MO
standard PCR primers
qPCR primers
spl-RNA
IR-RNA
C
% IR SNRNP70
50
40
30
20
10
0
control MO
SNRNP70 decoy MO
D
% IR SPTA1
30
20
10
0
control MO
SPTA1 decoy MO

Figure 5

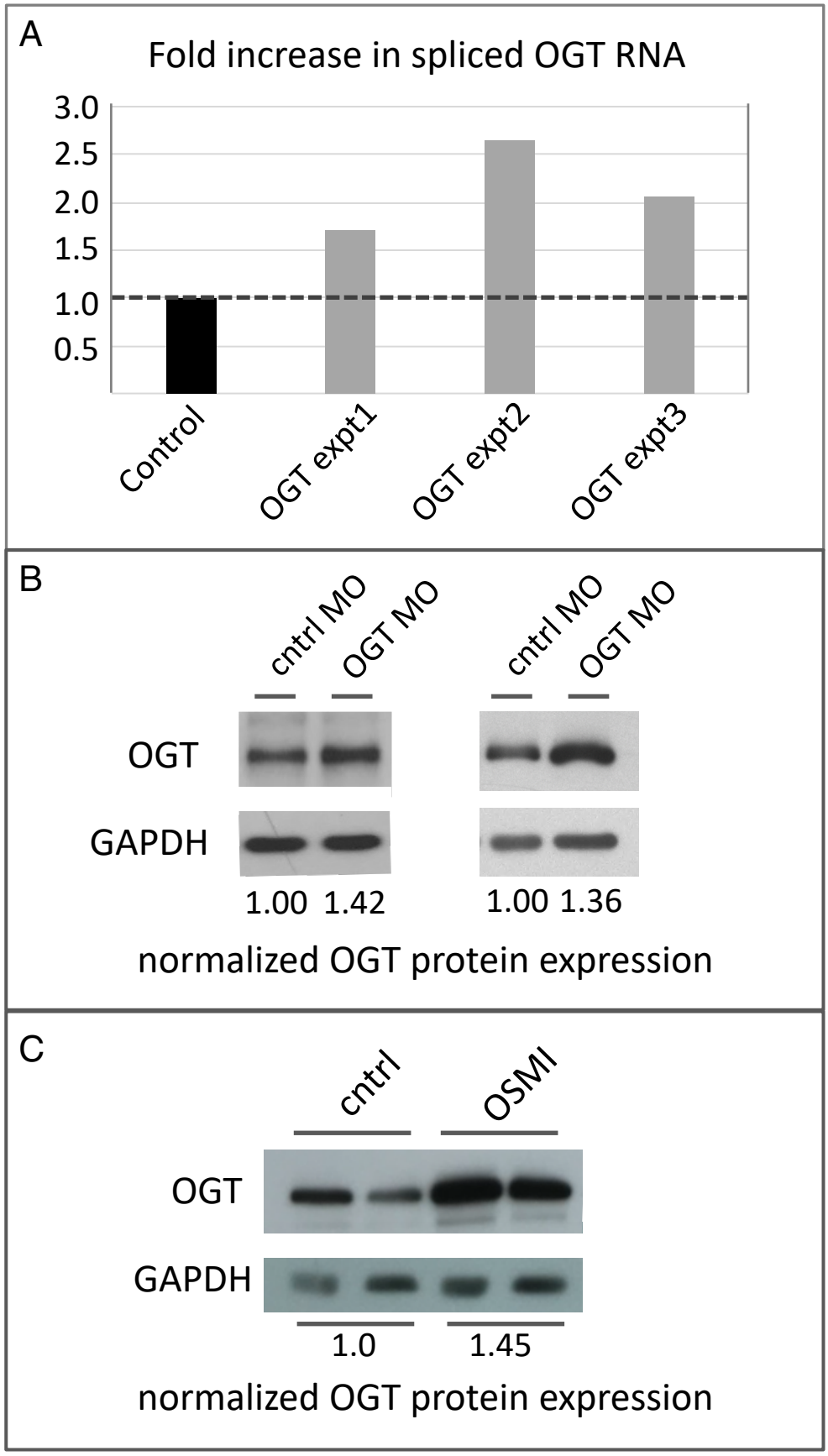
A
Fold increase in spliced OGT RNA
3.0
2.5
2.0
1.5
1.0
0.5
Control
OGT expt1
OGT expt2
OGT expt3
B
cntrl MO
OGT MO
cntrl MO
OGT MO
OGT
GAPDH
1.00 1.42
1.00 1.36
normalized OGT protein expression
C
cntrl
OSMI
OGT
GAPDH
1.0
1.45
normalized OGT protein expression

Table 1

Product	Size(nt)	primer location and sequence		
SF3B1-spl	138	forward	E4/5F	TCTTGATCCTTTTGCAGATGGAGG
		reverse	E6R	GCTTTAGCTTTTTCTGCTAGCTGTTG
SF3B1-IR	173	forward	i4F	GGCAGATAAATCAGTTGAACCTGC
		reverse	E5/6R	GCTGTTGCCTAATTTCTCGTTCTTC
OGT-spl	159	forward	E3/4F	TCTGCTCTTCAGTACAATCCTGATTTG
		reverse	E5R	AACACAGCCAAGATTACTCCAAG
OGT -IR	171	forward	E3/4F	TCTGCTCTTCAGTACAATCCTGATTTG
		reverse	i4R	GCTCAATGAAGAGTTGAAGACTTGG
SNRNP70-spl	149	forward	E7/8F	AGCGAGACATGCACTCCGC
		reverse	E9R	CCCTCCTCTTCTGGTACCAC
SNRNP70-IR	178	forward	i7F	CAGTTGCCTGGCTGTCTGTT
		reverse	E8R	CCATCAATCTTCTTGCCATCTGC
SPTA1-spl	191	forward	E20F2	ACAGTATGAAAGCTCTGCGGAATCAG
		reverse	E21/22-R2	CTTCCACCTTCCACCAGTCCTTA
SPTA1-IR	146	forward	E19/20F2	AGAAGCAGCTGGGGCTCTTC
		reverse	i20R2	GTGGGAAGTGTGAATCCTGTCATC
ACTB	187	forward	E4F	AGAGCTACGAGCTGCCTGAC
		reverse	E5R	AGCACTGTGTTGGGGTACAG
Products	**Size**	**primer location and sequence**		
SF3B1-IR SF3B1-spl	2.16kb 322nt	forward	E3F	CATCATCTACGAGTTTGCTTGG
		reverse	E6R	GCTGCTCCATTGACGACTTT
OGT-IR OGT-spl	3.65kb 380nt	forward	E3F	ACATGCATTGCGTCTCAAACC
		reverse	E6R	TGCGTGCCTCTTTCAAGACA
SPTA1-IR SPTA1-spl	2.06kb 249nt	forward	E19F	CAGCAGTACCTGGCTGACCT
		reverse	E21R	AGCCATGACCCTTTGTTCT

Table legend. Upper part of the table represents primers used to amplify small products via RT-qPCR. Lower table represents primers used for standard RT-PCR. Primer designations: E, exon; i, intron; F, forward; R, reverse. The symbol "/" indicates a primer that overlaps two exons and can only amplify spliced transcripts.

Antisense targeting of decoy exons can reduce intron retention and increase protein expression in human erythroblasts

Marilyn K Parra, Weiguo Zhang, Jonathan Vu, et al.

RNA published online April 20, 2020